Polymer 50 (2009) 4080–4088

Contents lists available at ScienceDirect

Polymer

journal homepage: www.elsevier.com/locate/polymer

Influence of structural organization on tensile properties in mesomorphic isotactic polypropylene

Koh-hei Nitta [a,*], Kazunari Odaka [b]

[a] Department of Chemical and Material Engineering, Institute of Science and Engineering, Kanazawa University, Kanazawa, Ishikawa 920-1192, Japan
[b] School of Materials Science, Japan Advanced Institute of Science and Technology, Japan

ARTICLE INFO

Article history:
Received 9 January 2009
Received in revised form
4 June 2009
Accepted 20 June 2009
Available online 26 June 2009

Keywords:
Isotactic polypropylene
Mesomorphic phase
Mechanical properties

ABSTRACT

The effects of annealing on the structure and mechanical properties of mesomorphic isotactic polypropylene have been investigated using wide-angle and small-angle X-ray scattering and rheo-optics in addition to tensile tests. Young's modulus of mesomorphic phase was estimated to be 5 GPa using Takayanagi model. The α-crystallitic iPP prepared by annealing the quenched mesomorphic iPP was transparent because of the absence of spherulitic structure. It was found that the mechanical yielding of α-crystallitic iPP is dominated by the plastic flow of crystalline structural units whereas the yield process of α-spherulitic iPP quenched at 80 °C is caused by the fracture or fragmentation of crystalline structural units.

1. Introduction

It is well known that isotactic polypropylene (iPP) is a typical polymorphic material with three main crystal forms such as monoclinic α-modification, hexagonal β-modification, and triclinic γ-modification in which the α-form crystal is the most stable crystalline forms in iPP [1]. In addition, iPP with an intermediate order between crystalline and amorphous phases is obtained on rapid cooling from the melt. Natta et al. [2] termed this structure the "smectic" state and suggested that the smectic structure is composed of parallel 3/1 helices similar to α-modification but the disorder exists in the packing of the chains perpendicular to their axes. Here we call it "mesomorphic phase or mesophase". The mesophase can be considered as a frozen intermediate ordering state during crystallization which is caused by a quenching solidification process which hinders molecular motions necessary for crystallization [3]. Although this quenched phase is stable at room temperature, it transforms to the monoclinic α-modification by heating at a temperature higher than 60 °C [4]. This structural transformation has been widely studied by a variety of structural characterization methods [5–10] such as differential scanning calorimetry (DSC), wide-angle X-ray diffraction (WAXD), small-angle X-ray scattering (SAXS), and transmission electron microscopy (TEM). Qui et al. [11] investigated changes of structure and morphology of quenched iPP films during tensile deformation at room temperature by synchrotron SAXS/WAXD techniques and found that the mesomorphic structure does not transform into crystal phase during deformation and the chains in the mesophase domains become highly oriented while keeping the 3/1 helical conformation in the yielding and necking regions. Ran et al. [12] showed that the α-from crystals are converted to the mesomorphic form with uniaxial drawing at room temperature. This kind of mesophase, that is deformation-induced mesophase, appears to be similar to the quench-induced mesophase form but they are essentially different because the latter is highly oriented with no SAXS long range ordering while the former is isotropic with an obvious SAXS long a range ordering as suggested by Qui et al. [11].

It is well known that slow cooling the molten iPP leads to spherulitic structure where α-crystalline lamellae are radially organized. The spherulitic structure is a typical macroscopic superstructure for various semicrystalline polymers and can be readily visualized by polarizing optical microscopy. It has been identified [10] that usual annealing process perfects the crystal structure but does not change the macroscopic morphological organization such as spherulites. It follows that annealing the mesomorphic structure converts to the nonspherulitic morphology with highly crystalline α-monoclinic form [4]. Olf et al. [13] compared stress-crazing of mesomorphic iPP, nonspherulitic α-crystalline iPP, and spherulitic α-crystalline iPP, showing that crazing behavior of the mesomorphic iPP and the nonspherulitic α-iPP is very similar to that of typical amorphous glassy polymers where the crazes are straight and strictly perpendicular to the stress direction whereas the spherulitic

* Corresponding author.
E-mail address: nitta@t.kanazawa-u.ac.jp (K.-h. Nitta).

0032-3861/$ – see front matter © 2009 Elsevier Ltd. All rights reserved.
doi:10.1016/j.polymer.2009.06.050

iPP crazes an entirely different manner from glassy polymers, showing that crazing happens that a craze zigzags from center to center through several spherulites. O'Kane et al. [14] investigated the effects of annealing on the structure and tensile properties of α-monoclinic structure and the quenched mesomorphic structure. They found that the yield stress strongly depends on the size and perfection of the crystalline regions.

A number of works have been conducted on morphology transformation and deformation behaviors of mesomorphic iPP. However, few works have been done to systematically investigate the comparison of tensile properties among mesomorphic, non-spherulitic, and spherulitic iPP materials. The purpose of this study is to investigate the dependence of the tensile properties of the quenched iPP on the structural changes induced by the annealing process. In addition, we compared the mechanical properties of these annealed iPP with those of typical spherulitic iPP which were prepared by quenching at a higher temperature. For example, in the case of injection molded iPP materials the skin phase in the iPP materials form a quenched structure while their core phase is slowly cooled. Thus, the morphology of the iPP materials is significantly complicated and is mixture of quenched and slow-cooled structures. Therefore, it is very important to examine the dependence of the tensile properties of iPP on the structural changes induced by the annealing and cooling process.

2. Experimental

2.1. Materials

Material used in this work is a commercial iPP with a high tacticity (98–99%), weight average molecular weight M_w of 260 k and a polydispersity of $M_w/M_n = 5.7$. The iPP pellets were compression molded in a laboratory hot press at 230 °C. The samples were completely melted for 15 min between two aluminum sheets prior to the application of a pressure of 10 MPa to produce iPP sheets of about 200 μm thickness. On removal from the press, the samples were plunged directly into an ice water bath maintained at 0 °C to prepare the mesomorphic iPP sheets. The degree of transformation to the monoclinic α-form was controlled by changing the annealing temperature from 25° to 140 °C. The structural characteristics of these samples are presented in Table 1. A series of these iPP samples (sample code C) showed no spherulitic structure and the end-numeral of code C denotes the quenching temperature in °C. In particular, we call the C140 sample "crystallitic iPP" in this paper.

For comparison, we prepared α-spherulitic iPPs by quenching at 80 °C after being melted in the hot press. The crystallinity of the spherulitic iPPs was controlled by changing the annealing temperature from 80° to 140 °C. The structural characteristics of these samples (the sample code S) were listed in Table 2. The end-numeral of sample code S denotes the quenching temperature in °C.

Table 1
Structural characteristics of annealed mesomorphic iPP samples.

Sample	Anneal temp./°C	Density/ kg m^3	ϕ_α/%	ϕ_{meso}/%	ϕ_{amor}/%	L_p/nm	L_c/nm	L_m/nm	L_a/nm
C25	25	881	0	43.5	56.5	8.67	0	3.77	4.90
C40	40	884	0	48.4	51.6	8.93	0	4.32	4.61
C60	60	886	0	51.6	48.4	9.68	0	4.99	4.69
C80	80	894	20.6	37.4	42.0	10.8	2.22	4.04	4.54
C100	100	901	42.4	20.3	37.3	13.1	5.55	2.66	4.89
C120	120	906	52.3	14.4	33.3	15.3	8.00	2.20	5.09
C140	140	910	68.3	0	31.7	18.9	12.9	0	5.99

ϕ_α: fraction of α-crystal/ϕ_m: fraction of mesophase/ϕ_α: fraction of amorphous/L_p: long period/L_c: crystalline thickness/L_m: mesophase thickness/L_a: amorphous thickness.

Table 2
Structural characteristics of spherulitic iPP samples.

Sample	Anneal temp./°C	Density/ kg m^3	ϕ_α/%	ϕ_{meso}/%	ϕ_{amor}/%	L_p/nm	L_c/nm	L_m/nm	L_a/nm
S80	80	901	57.3	0	42.7	12.1	6.93	0	5.17
S100	100	906	63.4	0	36.6	14.0	8.88	0	5.12
S120	120	908	65.9	0	34.1	16.1	10.6	0	5.49
S140	140	910	68.3	0	31.7	17.9	12.2	0	5.67

ϕ_α: fraction of α-crystal/ϕ_m: fraction of mesophase/ϕ_α: fraction of amorphous/L_p: long period/L_c: crystalline thickness/L_m: mesophase thickness/L_a: amorphous thickness.

2.2. Measurements

2.2.1. Tensile measurements

Dumbbell-shaped specimens were used for the tensile tests. They were cut from the compression molded sheets of 200 μm thickness with a cutter and have a gauge length of 10 mm and a width of 4 mm. The samples were elongated at room temperature (25 °C) and at a constant elongation speed of 1, 5, 10, 20, 50, and 100 mm/min using a Shimadzu AGS-5kN. The tensile stress was determined from dividing the tensile load by the initial cross-section and the tensile strain was calculated from the ratio of the increment of the length between clamps to the initial gauge length.

In addition, the thickness and width of the sample specimens were measured under tensile deformation in order to estimate the Poisson's ratio. For the purpose, a Keyence LS-3100 and LS3034 laser detectors were mounted on the AGS tensile machine. The elongation speed was 2 mm/min. The rectangle specimens with 200 μm thick, 20 mm width, and 40 mm length were used for the measurements.

2.2.2. Rheo-optical measurements

In this work, infrared dichroism was measured simultaneously with tensile deformation at a constant speed of elongation to investigate the chain orientation behavior. A tensile tester was set in Fourier-transform infrared spectrometer (ORIEL MIR8000) in such a way to allow infrared beam through a film specimen mounted on the tensile tester. The tensile tester was specially designed for upper and lower clamps to symmetrically move from the central point of the film so that the beam spot remains at the initial position during a whole stretching. The elongation speed was 1 mm/min in all cases. Double-edge-notched specimens with a gauge length of 4 mm, a ligament length of 4 mm, a width of 16 mm were used for the tensile tests. They were punched out from compression-molded films of 100 μm thick.

In order to quantitatively examine the stress-whitening under tensile deformation, we measured the transmission intensity of visible light (wave length = 632.8 nm) during tensile deformation. For the purpose, the tensile tester described above was mounted on an optical system SALS-100S (IST Planing Co.) in which the 2 mW He–Ne laser beam is rendered perpendicular to the stretching direction, passes through the center (stressed region) of the specimen and into a photomultiplier. The transmitted intensity was recorded by a transient computer memory as a function of time. The elongation speed was fixed to be 1 mm/min.

2.3. Characterization

The WAXD measurements were carried out at room temperature with a Rigaku RU-200 diffractometer with Ni-filtered Cu-Kα radiation from a Rigaku generator operated at 40 kV and 100 mA at a scanning rate 2°/min over the diffraction angle 2θ range from 10 to 25°. As shown in Fig. 1, the diffraction patterns of all the samples have a broad amorphous background superimposed on five sharp

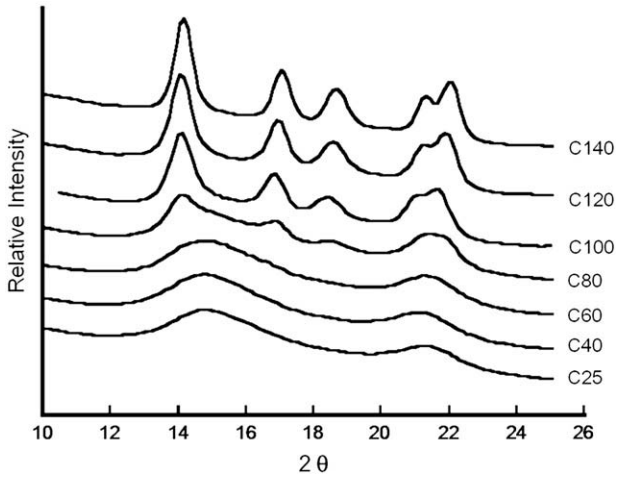

Fig. 1. WAXD patterns of annealed mesomorphic iPP sheets. The details of samples are listed in Table 1.

diffraction lines ascribed to the 14.1, 16.9, 18.5, 21.8, and 22.1° for α-modification and/or to the 14.5 and 21.5° for mesomorphic modification. The degree of transformation from mesomorphic to α-modification increases with the annealing temperature.

On the basis of the analysis method proposed by Martorana et al. [15], we estimated the volume fraction of mesophase in the non-amorphous part. Because the WAXD reflection peaks of α-crystalline, mesomorphic, and amorphous components are overlapped for the present iPP samples, curve-fitting processing by using the Gauss function was carried out to separate the WAXD peaks and their integral areas were computed. In the WAXD profile, (110) at $2\theta = 14.1°$, (040) at 16.9°, (130) at 18.5° are principal reflections of the α-crystals of iPP whereas the peak at 14.5° is the principal reflection of mesophase, and they are considered as the markers for α-crystals and mesophase, respectively. The various reflection areas were computed after subtraction of the amorphous halo. The mesophase fraction in the crystalline part of any specimen was assessed from the ratio of the area of the main mesophase reflection at 14.5° (S_{meso}) to the sum of the total area of the main crystalline reflections ($S_\alpha = S_{\alpha1} + S_{\alpha2} + S_{\alpha3}$) such as a (110) at $2\theta = 14.1°$ ($S_{\alpha1}$), (040) at 16.9° ($S_{\alpha2}$), and (130) at 18.5° ($S_{\alpha3}$) from the α phase plus reflection from the mesophase (S_{meso}).

Densities of the films were determined by a flotation method at room temperature. The binary medium prepared from various ratios of distilled water and ethyl alcohol was used. Assuming that mesophase regions consists of liquid-like lateral disorder with imperfect *c*-axis registration [16], the volume fraction of amorphous phase ϕ_a was determined from the density data using

$$1 - \phi_a = \frac{\rho - \rho_a}{\rho_c^* - \rho_a} \quad (1)$$

where ρ is the overall density of the sample, ρ_a is the density of amorphous phase which are taken to be 854 kg/m^3 [17], and ρ^*_c is the density of non-amorphous phase given by the following equation:

$$\rho_c^* = r\rho_{meso} + (1 - r)\rho_\alpha \quad (2)$$

where ρ_α is the density of α-crystal which is 936 kg/m^3 [18], ρ_{meso} is the density of mesophase which is 916 kg/m^3 [19], and r is the volume fraction of mesophase in the non-amorphous part which was determined by the weight fraction of each phase estimated from using the above WAXD method in addition to the density of each phase. The volume fractions of α-crystal phase ϕ_α, mesophase ϕ_{meso}, and amorphous ϕ_a estimated using Eqs. (1) and (2) were listed in Tables 1 and 2. In Fig. 2, each fraction is plotted against the annealing temperature. The amorphous phase monotonously decreases with increasing the annealing temperature. It was suggested that the mesophase is transferred into α-crystal form by annealing at higher temperatures above 60 °C according to the literature [3] and a part of amorphous is converted to the mesophase by annealing at lower temperatures below 60 °C.

The SAXS measurements were performed with a point focusing optics and a one-dimensional position sensitive proportional counter (PSPC) with an effective length of 10 cm. The Cu-Kα radiation supplied by a MAX Science M18X generator operating at 40 kV and 30 mA was used. The SAXS profiles of C- and S-samples are shown in Fig. 3. The inverse of the SAXS peak position on Iq^2 versus q curve (Lorentz-corrected SAXS curve) yields the long period L_p. As shown in these figures, the annealing of C- and S-samples leads to an increase in the SAXS long period. In addition, the SAXS profile of C-samples exhibited broader and less intense than those of S-samples but the annealing process changes the broad peak in SAXS profile of quenched iPP (C-samples) to reach the sharp patterns of spherulitic iPP samples (S-samples).

Assuming that the mesophase is the partially disordered α-form and/or in the paracrystalline state [20], three or two-phase model can be employed and the thickness of α-crystalline lamellae, mesophase and amorphous layer can be estimated from the product of their volume fractions and the SAXS long period values. These analytical data are listed in Tables 1 and 2.

The formation of supermolecular structure such as spherulites can be revealed by transmission optical microscope between crossed polarizers. The pictures of C25, C140 and S140 are exemplified in Fig. 4. It was confirmed that S140 sample is typical spherulitic whereas there are no supermolecular structure in C-samples being independent of the degree of transformation to α-modification. In addition, these pictures suggest that C-samples show a high transparency whilst α-spherulitic iPP samples were not clear because of the light-scattering due to the spherulitic structure. The heat-treatment of quenched iPP can be considered to be a practical method for preparing a transparent α-iPP film.

TEM measurements were done with a HITACHI H-7100 transmission electron microscope applying an acceleration voltage of 80 kV. The ultrathin specimens were sectioned into slices of about 100 nm thickness with an ultramicrotome (Reichert-Nissei ULTRACUTS) at −140 °C. The ultrathin films were then stained with ruthenium tetraoxide. Photographic contrast is produced by selective electron scattering from the stained non-crystalline phase. As

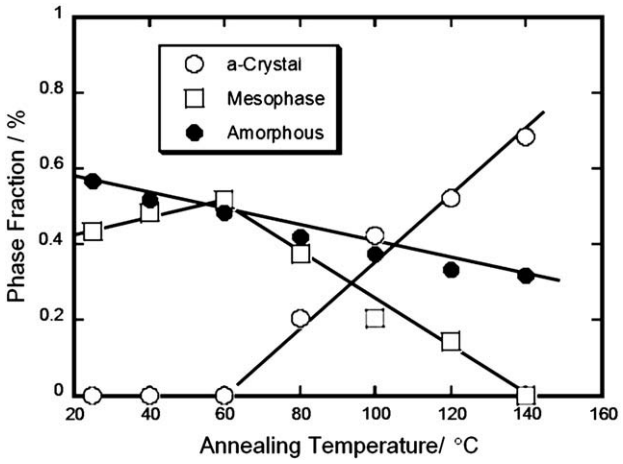

Fig. 2. Phase fraction plotted against the annealing temperature of C samples.

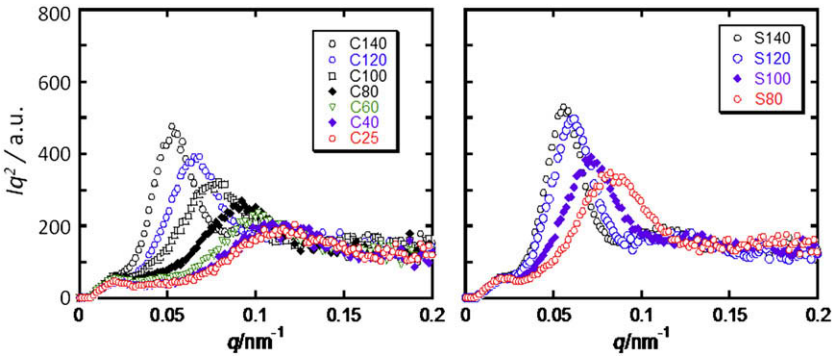

Fig. 3. SAXS patterns of crystallitic iPP (C) and spherulitic iPP (S) samples.

shown in Fig. 4, TEM pictures also demonstrate that the annealing iPP quenched at 0 °C exhibits no significant supermolecular structure whereas the iPP quenched at 80 °C exhibits typical spherulitic structure the size of which was about 20–30 μm. In addition, the fibrils with thickness of 200–500 nm, which appears be composed of bundles of stacked lamellar clusters as demonstrated by Nitta–Takayanagi [21], were found to radiate from the center of spherulites.

3. Results and discussion

Fig. 5 shows the stress–strain curves at room temperature for C-samples with different mesophase contents. The overall stress levels are increased by transformation of mesophase to monoclinic α-form. The yield peak of mesomorphic iPP is significantly broad and it becomes narrower and much intense as the fraction of α-crystalline phase increases.

Young's moduli estimated from these stress–strain curves are listed against the annealing temperature. The Young's moduli of these iPP samples having a variety of structural organization were analyzed using a multi-component Takayanagi model [22] as shown in Fig. 6. In the model A is the major component and the dispersed component B is composed of two parts: B2 is the minor component and B1 is the intermediate component. If the sample is a two-phase system, B2 is set to be B1 and the model corresponds to a typical Takayanagi model.

In the case of two-phase model that a part of the A component is coupled in parallel with the B component and the remainder of A is coupled in a series with the A–B parallel element, the modulus E is given by

$$E = E_A \frac{\left(1-\sqrt{\phi_B}\right)E_A + \sqrt{\phi_B}E_B}{\left(\phi_B + 1 - \sqrt{\phi_B}\right)E_A + \sqrt{\phi_B}\left(1-\sqrt{\phi_B}\right)E_B} \tag{3}$$

where E_A is the modulus of the A component, E_B is the modulus of the B component, and the ϕ_B is the fraction of the B component. This equation was derived under an assumption that the material is mechanically isotropic. In the multi-component model, the component B is composed of B1 and B2 parts in which a part of the B1 component is coupled in parallel with the B2 component and the remainder of B1 is coupled in a series with the B1–B2 parallel element. In this multi-component model, the modulus of E_B is given by

$$E_B = E_{B1} \frac{\left(1-\sqrt{\phi'_{B2}}\right)E_{B1} + \sqrt{\phi'_{B2}}E_{B2}}{\left(\phi'_{B2} + 1 - \sqrt{\phi'_{B2}}\right)E_{B1} + \sqrt{\phi'_{B2}}\left(1-\sqrt{\phi'_{B2}}\right)E_{B2}} \tag{4}$$

where E_{B1} is the modulus of the B1 component, E_{B2} is the modulus of the B2 component, and the ϕ'_{B2} is the fraction of the B2

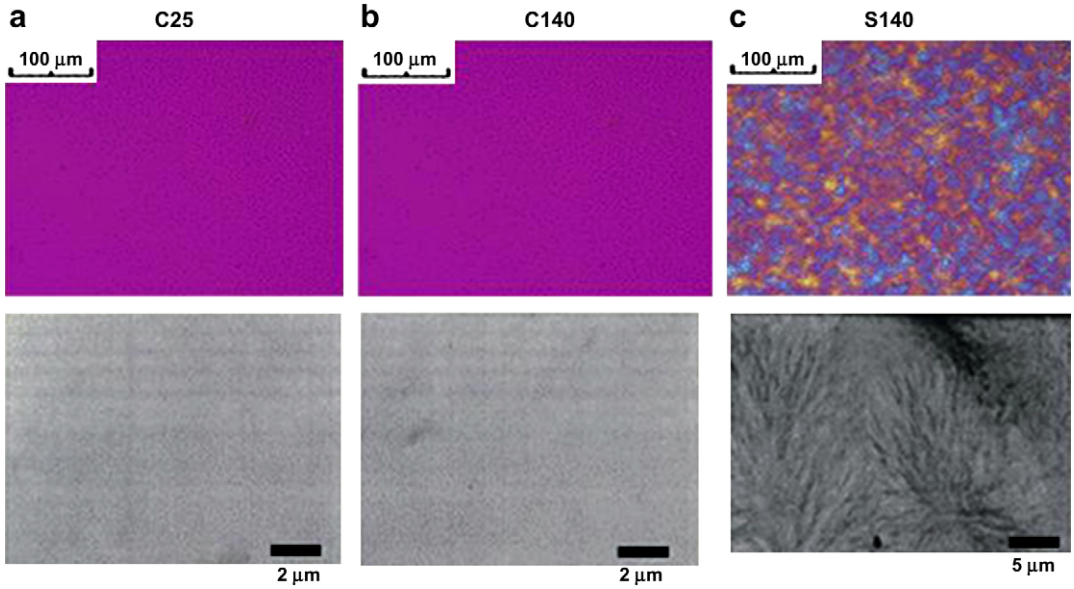

Fig. 4. Polarized optical microscope and TEM pictures of iPP samples: S25 (mesomorphic iPP), S140 (crystallitic iPP), and S140 (spherulitic iPP).

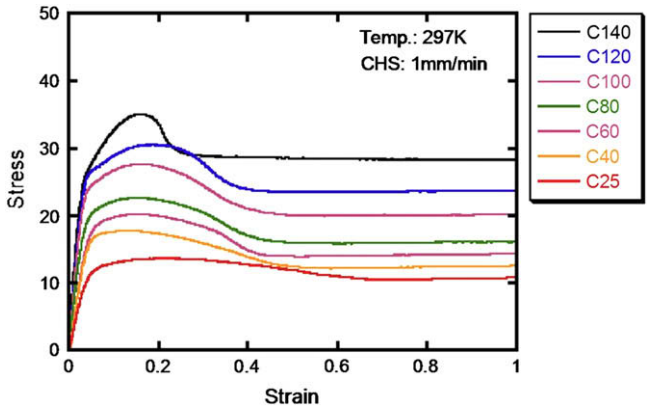

Fig. 5. Stress–strain curves measured at 25 °C and a cross-head speed of 1 mm/min of C-samples.

component in the B element and given by ϕ_{B2}/ϕ_B where ϕ_{B2} is the fraction of the B2 component in the multi-component model. The modulus of the multi-component model can be obtained by putting Eq. (4) into Eq. (3).

In this work, the modulus of α-crystal phase E_α was taken to be a theoretical value of 45 GPa [23]. Fitting the two-phase Takayanagi model to experimental data of a set of α-spherulitic iPP (S-samples) yields Young's modulus of amorphous phase $E_{amor} = 0.15$ GPa. Using these values $E_\alpha = 45$ GPa and $E_{amor} = 0.15$ GPa, the modulus of mesophase E_{meso} was estimated to be 5 GPa by fitting the multi-component Takayanagi model to the experimental data of C-samples. Table 3 compares between the experimental Young's moduli and the computational ones.

As shown in Tables 1 and 2, C140 and S140 samples are α-crystalline iPP samples and have the similar lamellar morphology or crystallinity but C140 has no spherulites (α-crystallitic) and S140 is

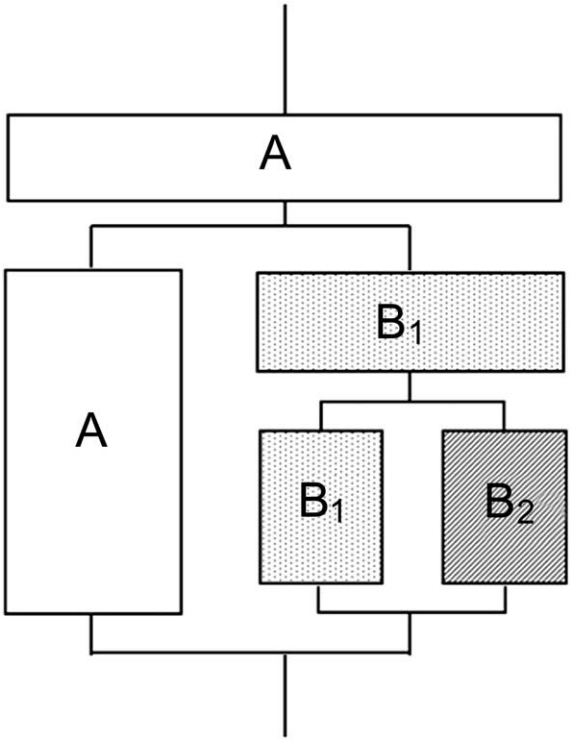

Fig. 6. Multi-component Takayanagi model.

Table 3
Young's modulus.

C140		S140	
Exp.	Calc.	Calc.	Exp.
0.39	0.40	0.68	0.60
0.45	0.45	0.73	0.72
0.44	0.48	0.78	0.79
0.60	0.59	0.82	0.84
0.69	0.69		
0.72	0.79		
0.87	0.85		

α-spherulitic. Fig. 7 compares the stress–strain curves of C140 and S140 which has the same crystallinities of 68.3%. In the initial strain region up to about 0.03 of strain where the stress is proportional to the strain, there is no difference in stress–strain curve. Thus, these samples delineate the same stress–strain curve in the initial strain region. The insensitivity to the spherulitic structure is theoretically confirmed by this author [24,25]. In other words, the present results are consistent with our previous conclusion that the deformation of the amorphous phases dominantly affects the modulus and the stress level in the initial strain region [25]. This will be due to the fact that the external load is concentrated on the amorphous region because the rigidity of crystalline phase is much greater than that of amorphous region [24].

The crystallitic C140 sample has double yield peaks similar to polyethylene (PE) materials [26] whereas the spherulitic S140 has a sharpened yield peak. The necking appeared at around the second yield peak for C-series samples while the necking of spherulitic iPP samples was initiated beyond the yield point. The second yield peak was found to be pronounced by transformation of mesomorphic phase to α-crystal phase, indicating that the enhancement of the yield stress is a consequent of an increase in the perfection of the crystalline phase as suggested by O'Kane et al. [14]. Fig. 8 shows the dependence of the maximum (yield) stress on density for C- and S-samples. As was found for the C-sample data, the yield values fall onto two straight lines in the high and low density regions. This demonstrates that the yield mechanism is essentially different between the low density C-samples having no α-crystal phase, or transforming from the amorphous phase to the mesophase and the high density C-samples transforming from the mesophase to α-crystal phase. For the low density C-samples, the transformation from amorphous phase to mesophase enhances the maximum stress or yield stress. On the other hand, for the high density C-samples, the yield stress is increased by an increase of the crystal content or crystallinity. It is interesting to note that the yield

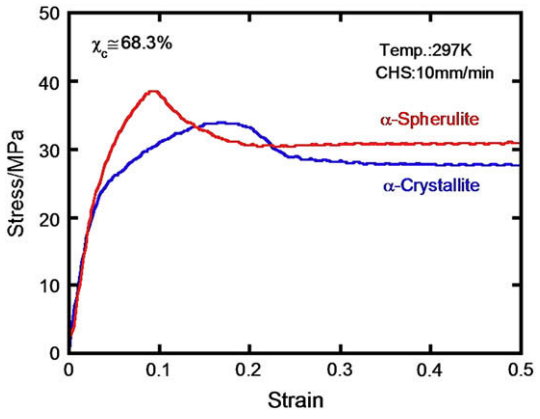

Fig. 7. Stress–strain curves measured at 25 °C and a cross-head speed of 10 mm/min of crystallitic iPP (C40) and spherulitic iPP (S140) having a fixed crystallinity of 68.3 vol%.

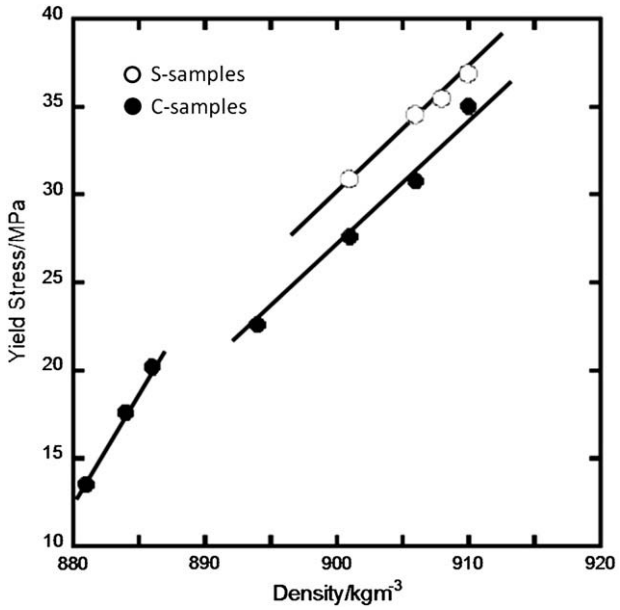

Fig. 8. Yield stress plotted against density data. The open circle denotes the S samples and the closed circle denotes the C samples.

values of C- and S-samples fall on the different lines which are parallel to each other, and the spherulitic iPP samples show a higher yield stress as compared with the crystallitic iPP samples.

The linear relation between the density and the yield stress has been identified for linear PE [27]. The same slope of the both lines of the S-samples and high density C-samples suggests that the origin of yield process is the same with each other and the yield process is predominantly associated with the irreversible deformation of crystalline phase. In other words, the high density C-samples as well as the S-samples can be treated as a semicrystalline polymer and their yield process is based on an analogy to the plastic deformation and dislocation of crystals as suggested by Bowden et al. [28]. The fact that the yield stress of the high density C-samples is less than that of S-samples may be attributed to a lack in the energy requirement for deformation and a large scale of re-organization of spherulitic structure. The change in the character of the yield stress of the low density C-sample is due to the fact that the lower-density C-samples are composed of mesophase and amorphous phase, and they cannot be treated to be as a typical semicrystalline polymer. The decrease in the yield stress with decreasing the density, or increasing the amorphous content, resembles the effects of the yield stress and overall stress level on elevating temperature, and the yield region for these samples is very diffuse as compared with that of the high density C-samples.

The dependences of the stress–strain curves in mesomorphic iPP (C25) and crystallitic iPP (C140) samples on tensile speeds are summarized in Fig. 9(a) and (b), respectively. The important results that are obtained from the major difference between these figures are that the overall stresses increase with increasing elongation speed and the first yield point is more pronounced for C25 while the second yield point is more pronounced for C140. Considering that C25 is mesomorphic and the mesophase region consists of smectic aggregation of helical chains which can be considered to be a loosely organized crystalline part and the interactions between helical chains are weak, the dominant factor for the yield process of mesomorphic C25 is likely to be the pulling-out processes of helical chains from the mesomorphic domains. Therefore the dependence of the yield behavior on elongation speed and temperature may be described by a thermally activated rate process [29]. On the other hands, the crystallitic C140 is a semicrystalline iPP so that the second yield process will be associated with the irreversible structural re-organization into oriented state. The deformation mechanism will be discussed later.

The effects of structural organization on the orientation behavior were examined using mesomorphic iPP (C25), crystallitic iPP (C140) and spherulitic iPP (S140). In this work, the intensity of 998 cm^{-1} band, which is ascribed to CH_3 rocking mode as coupled with C–CH_3 stretching mode, was measured as a function of time or strain every 1 s. Using the dichroic ratio of the band, we estimated the orientation function of crystal *c*-axis as described previously [30].

The yield peak of C25 is more diffuse and poorly defined. Following yield, a more pronounced upswing in the orientation function is observed for C25 as compared with crystalline samples such as C140 and S140 (see Fig. 10). The negative orientation in the pre-yield region as seeing in well-organized spherulitic S140 is due to the fact that the deformation of well-organized spherulites leading to the orientation of lamellae (or a^*-axis or *b*-axis) causes the *c*-axis to orient perpendicular to the stretching direction.

Fig. 11 illustrates the 2D WAXD patterns of the original and drawn films (with a fixed draw ratio of 2) of C25, C140, and S140. The WAXD patterns of original samples before drawing show that all samples are completely isotropic. Two broadened ring being associated with the mesomorphic phase are located for C25 (see Fig. 11(a)). The WAXD data of crystallitic C140 and spherulitic S140 showed the five strong rings of the α-form crystal, which can be attributed to the (110), (040), (130), (060), and (−131) reflections. The WAXD peaks of drawn films are azimuthally centered on the meridian, indicating oriented states. It should be noted here that the 2D-WAXD pattern of drawn C140 shows sharp diffraction peak while 2D-WAXD pattern of drawn S140 is broadened and is similar

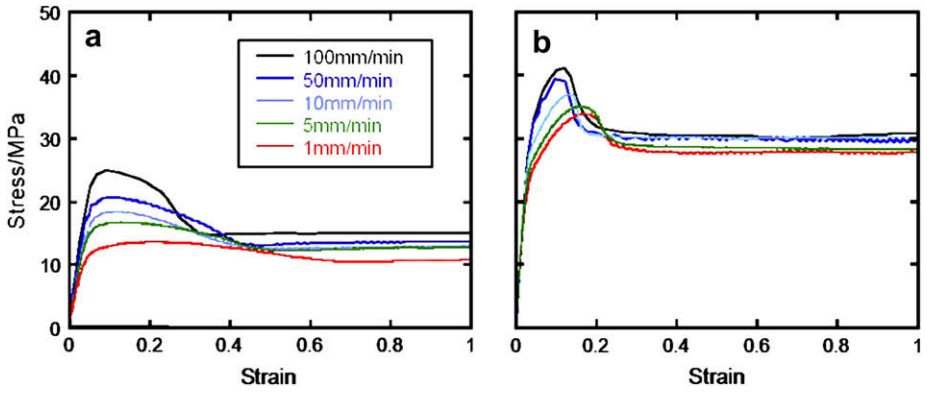

Fig. 9. The tensile speed dependences of the stress–strain curves measured at 25 °C for (a) mesomorphic iPP (C25) and (b) crystallitic iPP (C140) samples.

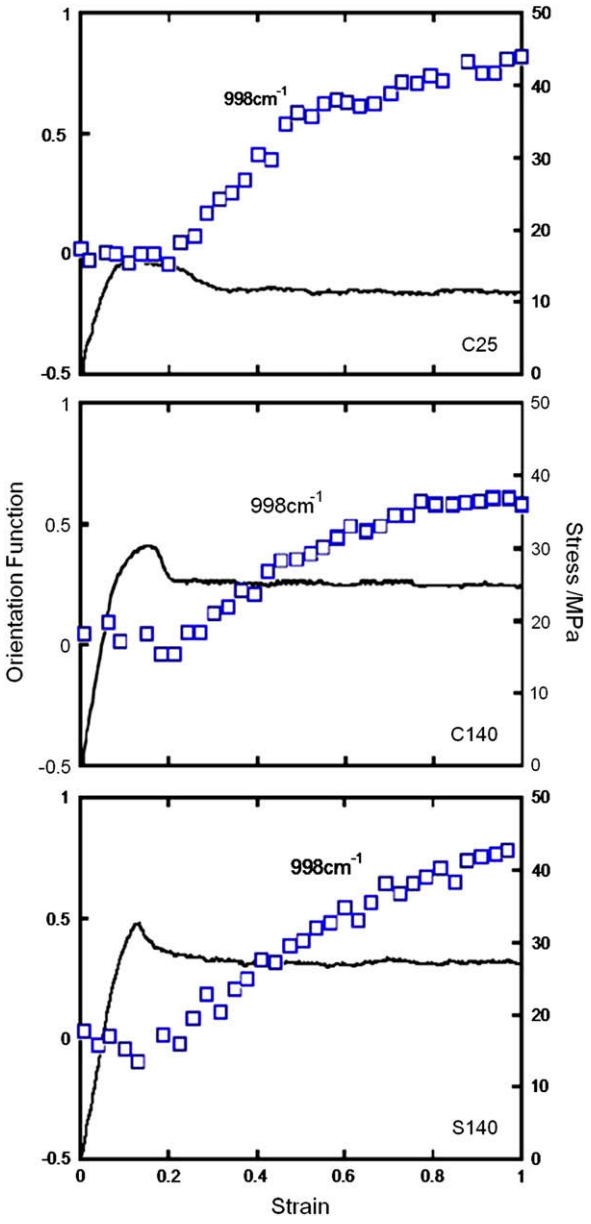

Fig. 10. Orientation function of crystalline axis (998 cm^{-1}) under a tensile test measured at 25 °C and a cross-head speed of 1 mm/min for mesomorphic iPP (C25), crystallitic iPP (C140), and spherulitic iPP (S140).

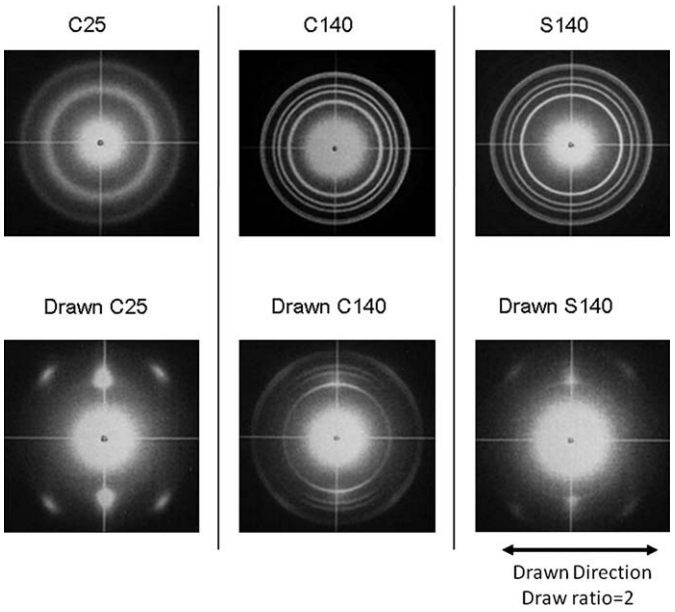

Fig. 11. WAXD diffraction patterns of original samples of C25, C140 and S140 and their draw samples at 2 of draw ratio.

to that of drawn mesomorphic structure, which could be due to two reasons: one is that crystals are disintegrated by the yield process and the other is that there is the evolution of the mesomorphic form caused by the chain-pulling from deformed crystalline structures as suggested by Ran et al. [12] The comparison of WAXD patterns between deformed C140 and S140 samples reveals that the yielding process in spherulitic structure diffuses the α-crystal structure.

It was found that some of specimens show stress-whitening during tensile deformation. The stress-whitening was easy to observe with eye but was difficult to characterize quantitatively. To obtain quantitative data of the stress-whitening, we measured the intensity of light transmittance under a tensile deformation. In Fig. 12, the transmitted intensity I normalized by the initial intensity of original film I_0 was plotted against strain together with stress–strain curves. The transmitted intensity of C25 and C140 suddenly dropped to zero just after yield process or at the neck initiation. Also, the transmitted intensity of S140 starts to decrease at around the yield initiation point and gradually becomes zero after yielding region. The decrease in light transmittance may be due to the light scattering caused by some entities such as micro-voids and cracks in the deformed specimen. It is interesting to note that for mesomorphic C25 films the intensity increases again during necking deformation and the transparency recovered in the necking process. It should be noted here that the drop of transmittance at the initiation of necking is considered to be caused by the light scattering due to a ramp surface between the necked and unnecked regions when the necked part is initiated within the laser spot. After extending the necked region all over the laser spot, the transmittance of C25 was recovered, indicating that there are no micro-voids and crack in the deformed C25.

Fig. 13 compares the strain dependences of the values of Poisson's ratio measured simultaneously with tensile tests between S140 and C140 samples. The Poisson's ratio of S140 has a maximum point at around 0.03 and decreases with increasing strain while that of C140 is almost constant under deformation. Considering that the decrease of Poisson's ratio may be associated with the volume expansion, various types of defects such as voids and cracks are caused by disintegration and fragmentation of crystalline phase for α-spherulitic iPP. The constancy of Poisson's ratio of C140 as well as the clear WAXD patterns in the drawn C140 led us to conclude that the plastic flow deformation dominantly takes place at yielding process without disintegration and fracture of crystalline phase. It was found that yield mechanism of C140 is much different from that of S140 and it is largely dependent of the presence of supermolecular structure.

The yielding process of semicrystalline polymers leads to a large scale of transformation from isotropic structure to fibrillar one brought about by the destruction of crystalline phase and molecular reorganization based on the plastic flow of crystalline chains. According to theoretical consideration of solidification process of spherulitic iPP materials by Nitta–Takayanagi [21], the clustering process of crystalline lamellae takes place under the super-cooled state. The precursor cluster units are evolved by the exclusion process of chain-ends during solidification, the inside of which

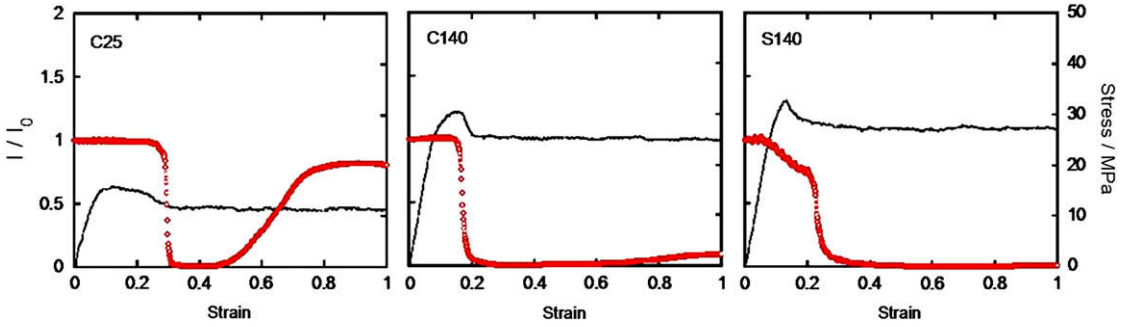

Fig. 12. Light transmittance intensity measured under a tensile test 25 °C and a cross-head speed of 10 mm/min for mesomorphic iPP (C25), crystallitic iPP (C140), and spherulitic iPP (S140).

includes some intertwining chains, and they are developed to lamellar clusters which are organized to be spherulitic morphology. It follows that the size of the cluster units corresponds to the end-to-end distance of polymers.

When the cluster units develop into the lamellar clusters, bundles of some extended tie molecules can longitudinally join together the adjacent cluster units belonging to the different lamellar clusters and bridge adjacent lamellar clusters. According to the previous theoretical treatments for yield deformation of spherulitic PE and PP materials [21], the intercluster links support the external force and their tractive forces act the cluster surface, leading a portion of the lamellar cluster to be bent around each intercluster link. At yield point, the fragmentation of lamellar clusters into the cluster units occurs and it can be considered to be accompanied by the dislocation and cleavage processes [31] of crystalline phases as demonstrated by Young [31].

Following this theoretical consideration, one possible hypothesis is that the mesomorphic iPP is composed of the loosely organized cluster units which are spinodally organized prior to be completely crystallized, leading to the density fluctuation of single-chain volume. In the case of crystallitic iPP, the precursor units are transformed into the stacked lamellar cluster units composed of well-organized α-crystalline lamellae by annealing process, resulting in that the cluster units with single chain-volume are not organized into spherulitic morphology but are randomly organized or loosely aggregated. The cluster units are connected by means of intercluster links to the neighboring ones which seems to correspond to the cluster-network model as proposed by Kilian [32].

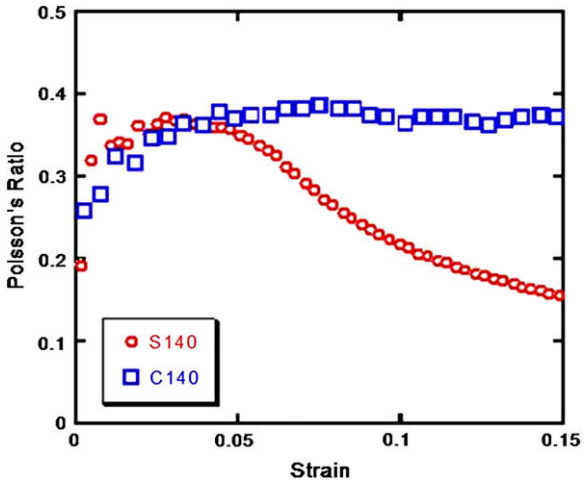

Fig. 13. Strain dependence of Poisson's ratio for crystallitic iPP (C140) and spherulitic iPP (S140).

As a consequent, it is suggested that when the crystallitic iPP sample is uniaxially stretched, the separation between the aggregated adjacent cluster units takes place at the first yield peak and the plastic flow and/or rotation process of the segregated cluster units to the stretching direction takes place at the second yield point, resulting in that the orientation of *c*-axis starts after the yield process. The long period and crystallinity of crystallitic iPP seems to mainly represent the inside structure of the cluster units. On the other hand, an external stress applied to the spherulitic iPP causes the cleavage between cluster units and decomposes the lamellar clusters within spherulites into fragments, i.e. cluster units at the yield point. After yielding, the decomposed cluster units orient to the stretching direction. The fragmentation of lamellar clusters into cluster units and the plastic flow of the fragmented units to the stretching direction are related to the initiation of necking beyond yield point [33]. Therefore, the diffuse WAXD pattern of a drawn spherulitic iPP and the decrease of Poisson's ratio around yield point will be associated with the volume expansion due to void-opening and cracks caused by the fragmentation and disintegration of lamellar clusters into cluster units. On the other hand, yielding of crystallitic iPP is mainly due to the plastic flow process of the segregated cluster units and needs not the cleavage process of crystalline phase between cluster units, resulting in that the WAXD profile of a drawn crystallitic iPP film in the necked region is very clear and its Poisson's ratio is almost constant under yield deformation.

4. Conclusions

We examined the effects of structural arrangement on tensile deformation of isotactic polypropylene. We compared the mesomorphic iPP prepared by quenched at 0 °C, the α-crystallitic iPP prepared by annealing the mesomorphic iPP, and α-spherulitic iPP prepared by quenched at 80 °C. The crystallitic iPP film was transparent because of the absence of spherulitic structure. The following conclusions have been drawn:

- Young's modulus is independent of the formation of spherulitic structure. Young's modulus of mesophase at room temperature was estimated to be 5 MPa which is an intermediate value between crystalline and amorphous phases.
- The volume expansion occurs during yield deformation for the spherulitic iPP while no excess volume-changes take place during yielding for the crystallitic iPP. It was suggested from the stress-whitening observation that the volume expansion is caused by the formation of micro-voids and crazes.
- The yield strength of mesomorphic iPP is much lower than that of the spherulitic and crystallitic iPP films. The mesophase is composed of loosely organized state of helical chains and the

yield process is based on the plastic flow of helical chains from the mesomorphic domains.

- The spherulitic iPP shows a sharp yield peak but the crystallitic iPP shows broad yield points, indicating that the yield process of spherulitic iPP is essentially different from that of crystallitic iPP: The yield deformation of spherulitic iPP is caused by the fragmentation of lamellar clusters into cluster units which is accompanied by the cleavage and dislocation of crystalline portions between cluster units. On the other hand, the yield deformation of crystallitic iPP follows the plastic flow of cluster units without the fragmentation of lamellar clusters.

References

[1] Bruckner S, Meille SV, Petraccone V, Pirozzi B. Prog Polym Sci 1991;16:361.
[2] Natta G, Corradini P. Nuovo Cimento 1960;15:40.
[3] Greblowcz J, Lau IF, Wunderlich B. J Polym Sci Polym Symp 1984;71:19.
[4] O'Kane WJ, Young RJ, Ryan AJ, Bras W, Debyshire GE, Man GR. Polymer 1994;35:1353.
[5] Vittoria V. J Macromol Sci Phys 1989;B28:97.
[6] Yan RJ, Li W, Li G, Juang B. J Macromol Sci Phys 1993;B32:15.
[7] Glotin M, Rahalkar R, Hendra P, Cuby M, Willis H. Polymer 1981;22:731.
[8] Finchera A, Zannetti R. Makromol Chem 1975;176:1885.
[9] Hsu CC, Geil PH, Miyaji H, Asai K. J Polym Sci Polym Phys 1986;24:2379.
[10] Gezovich DM, Geil PH. Polym Eng Sci 1968;8:202.
[11] Qiu J, Wang Z, Yang L, Zhao J, Niu Y, Hsia BS. Polymer 2007;48:6934.
[12] Ran S, Zong X, Fang D, Hsiao BS, Chu B, Phyllips RA. Macromolecules 2001;34:2569.
[13] Olf HG, Peterlin A. J Polym Sci Polym Phys 1974;12:2209.
[14] O'Kane W, Young RJ, Ryan AJ. J Macromol Sci Phys 1995;B34:427.
[15] Matorana A, Piccaralo S, Sapoindjieve D. Macromol Chem Phys 1999;200:531.
[16] Cohen Y, Saraf RF. Polymer 2001;42:5865.
[17] Jones AT, Cobbold J. J Polym Sci 1968;B6:539.
[18] Saqmuels J, Yee RY. J Polym Sci A-2 1972;10:385.
[19] Vittoria V. J Polym Sci Polym Phys 1986;24:451.
[20] Wyckoff HW. J Polym Sci 1962;62:83.
[21] Nitta K, Takayanagi M. J Macromol Sci Phys 2003;B42:107.
[22] Takayanagi M. Mem Fac Eng Kyushu Univ 1963;23:11.
[23] Sawatari C, Matsuo M. Macromolecules 1986;19:2653.
[24] Nitta K. Comput Theor Polym Sci 1999;9:19.
[25] Nitta K, Yamaguchi N. Polym J 2006;38:122.
[26] Brooks NW, Duckett RA, Ward IM. Polymer 1992;32:1872.
[27] Popli R, Mandelkern L. J Polym Sci Polym Phys 1987;25:441.
[28] Bowden PB, Young DY. J Mater Sci 1974;9:2034.
[29] Halsey G, White HJ, Eyring H. Text Res J 1945;15:295.
[30] Nitta K, Okamoto K, Yamaguchi M. Polymer 1998;39:53.
[31] Young RJ. J Mater Forum 1988;11:210.
[32] Kilian G. Colloid Polym Sci 1984;262:374.
[33] Nitta K, Takayanagi M. Polym J 2006;38:757.